Journal of Catalysis 418 (2023) 225–236

Contents lists available at ScienceDirect

Journal of Catalysis

journal homepage: www.elsevier.com/locate/jcat

In situ Raman spectroscopy study of silver particle size effects on unpromoted Ag/α-Al_2O_3 during ethylene epoxidation with molecular oxygen

Hashim A. Alzahrani, Juan J. Bravo-Suárez *

Center for Environmentally Beneficial Catalysis, The University of Kansas, Lawrence, KS, 66047, USA
Department of Chemical & Petroleum Engineering, The University of Kansas, Lawrence, KS, 66045, USA

ARTICLE INFO

Article history:
Received 14 September 2022
Revised 30 December 2022
Accepted 18 January 2023
Available online 21 January 2023

Keywords:
Silver
Alumina
Ethylene epoxidation
Structure sensitivity
Particle size
Crystallite
In situ Raman
Subsurface oxygen
Molecular oxygen

ABSTRACT

In situ Raman spectroscopy and parallel fixed bed reactor studies were conducted under ethylene epoxidation conditions with O_2 at 1 atm and 200 ℃ on unpromoted Ag/α-Al_2O_3 catalysts with different Ag particle sizes. It was found that for Ag particles of 20–50 nm, the weight normalized conversion rate decreased rapidly with increasing Ag particle size but remained almost constant above 50 nm. On the other hand, the apparent TOF increased with increasing Ag particle sizes in the 20–170 nm studied range, while ethylene oxide selectivity at zero residence time was nearly constant (55 ± 4%). Raman bands at 815 (all Ag sizes) and 880 (Ag sizes > 100 nm) cm^{-1} were identified and assigned to active molecular oxygen species. The 880 cm^{-1} species was assigned to a molecular oxygen complex structure stabilized by subsurface oxygen. The presence of the 880 cm^{-1} oxygen species likely explain the higher apparent TOF in larger Ag particles (>100 nm).

1. Introduction

Ethylene oxide (EO) is an essential cornerstone chemical in the petrochemical industry. It is the building block for many intermediates and products. The global EO production was 30 Mt in 2016 and is projected to reach 32 Mt by 2023 [1–3]. In 2018, only in the U.S., the production capacity of EO was 2.92 Mt, with a revenue of $3.4–3.9B/y. Around 72% of EO is consumed in the synthesis of glycols, primarily mono ethylene glycol (MEG) which is further polymerized to synthesize polyethylene terephthalate (PET) resin, the material from which most manufactured plastic containers are made of [4].

EO is selectively produced by reacting molecular oxygen with ethylene over Ag catalysts [5]. The unselective reaction path involves the high exothermic complete oxidation of ethylene and consecutive oxidation of EO to carbon dioxide. EO selectivities of unpromoted and promoted Ag/α-Al_2O_3 are around 40–50 % and 85–90%, respectively, at low ethylene conversions (<10%) to avoid extensive ethylene and EO combustion and for safety concerns [6,7]. In 2016, the total combustion of ethylene in the EO process corresponded to a loss of $2B/y [8]. Therefore, even slight improvements in EO selectivity would significantly enhance EO process economics while reducing CO_2 production. These environmental and economic drivers have motivated researchers to continue EO silver catalyzed process investigations despite its relative industrial maturity.

The industrial Ag/α-Al_2O_3 catalyst has a silver content of about 15–30% Ag with nanoparticles in the range of about 50–100 nm (and even larger) supported on a low surface area α-Al_2O_3 (<1 m^2/g) [7]. Overall, there have been multiple observations of significantly higher catalytic activity changes when the supported Ag particle size is increased between 10 and 100 nm [9]. This goes against the common intuition that on supported catalysts higher metal dispersion (small particle sizes) will usually favor catalytic activity for structure sensitive catalytic reactions. Such trends are widely reported in heterogeneous catalysis and therefore most supported catalysts are usually composed of metal nanoparticles <10 nm, whereas larger particles only possess a small fraction of active sites and are inefficient by behaving like bulk metals [10]. Thus, it is usually expected that for metal

* Corresponding author at: Center for Environmentally Beneficial Catalysis, The University of Kansas, Lawrence, KS 66047, USA ((J.J. Bravo-Suárez).
E-mail address: jjbravo@ku.edu (J.J. Bravo-Suárez).

https://doi.org/10.1016/j.jcat.2023.01.016
0021-9517/

nanoparticles>10 nm there should not be a significant change in catalytic activity [11–13]. The unusual structure sensitivity of silver catalysts for ethylene epoxidation was attributed by Boudart to surface saturation by possible impurities including various molecules and intermediates during preparation and pretreatment stages [11]. An evidence for that hypothesis was Campbell's observations showing similar turnover frequencies on Ag(1 1 1) and Ag (1 1 0) [14]. Hensen and co-workers recently suggested that the observed structure sensitivity may be related to the reported bulk structure of Ag particles [15,16]. Large particles consist of multiple joined crystallites separated by grain boundaries, presumably providing low resistance paths through which oxygen can diffuse from the bulk to the subsurface region and eventually to the silver surface to react with ethylene which may explain their higher turnover frequencies.

The silver catalyst for EO industrial production uses an α-Al_2O_3 support which has a low specific surface area (<1 m^2/g), and is nonporous [17,18]. During epoxidation reaction at temperatures between 200 and 300 ℃ the silver particle size can change via sintering due to the high silver loading and low support surface area [19–21]. Therefore, comparing particle size effects from various studies that utilized different reaction temperatures is not straightforward since the initial particle size distribution could change. One approach to minimize silver sintering is the use of a high surface area α-Al_2O_3 [12], but this approach might introduce support side effects on the reaction rate since EO can undergo secondary reactions with alumina's hydroxyl groups if the surface area (>8 m^2/g) or ethylene conversion are too large. This is the case for large surface area α-Al_2O_3 since EO can isomerize to acetaldehyde on the support's hydroxyl groups [22–24]. Low density of hydroxyl groups and specific surface area are the properties that make α-Al_2O_3 particularly useful for maintaining high EO selectivity [23,25,26], but at the expense of having low Ag dispersity. Furthermore, acetaldehyde formed by EO isomerization will combust rapidly to CO_2 over silver, which complicates the study of particle size effects on catalytic activity and selectivity [27].

The mechanism of ethylene partial and total oxidation remains debated despite almost a century of research [28–30]. In the heterogeneous catalysis route, it is expected that oxygen adsorbs on the Ag surface. Oxygen species were first suggested to be adsorbed molecular oxygen and atomic oxygen and presumed to be responsible for EO and CO_2 formation, respectively [31]. This proposal implied a maximum selectivity of 86% based on the reaction stoichiometry [32]. Later studies disputed this theory by confirming: (1) the desorption of molecular oxygen at temperatures significantly below reaction conditions [14,33,34] and (2) reporting EO selectivities higher than 86%. Some computational and spectroscopic studies have provided evidence that the active intermediate oxygen species in the reaction may be a chemisorbed atomic oxygen on Ag surface (O_α). It has also been proposed that the nature and bonding strength of these oxygen species to Ag surface dictate the reaction mechanism [35,36].

Moreover, two types of atomic oxygen have been postulated to be involved in the reaction, a weakly bonded atomic oxygen also called "electrophilic oxygen" (O_{elec}) or covalent oxygen and a strongly bonded oxygen also called "nucleophilic oxygen" (O_{nucl}) or ionic oxygen [37,38]. The O_{elec} is an electropositive charged species ($O^{\delta+}$) whose formation requires strongly positively charged Ag atoms with a low coordination number created by the presence of subsurface oxygen O_γ or surface defects [35,36]. The nucleophilic oxygen is suggested to be a surface oxide like Ag–$O^{\delta-}$–Ag (bridged oxygen) [39] species formed on Ag sites with low oxygen coverage, where charge transfer from Ag to adsorbed oxygen creates silver cations Ag^+ necessary for ethylene adsorption [40]. Based on earlier isotope experiments [29,41] and recent DFT calculations [12,30,42–44], it is believed that O_{nucl} attacks the C–H bond to form CO_2 whereas O_{elec} is responsible for the electrophilic attack of the π bond in ethylene, creating an adsorbed epoxide cycle intermediate called oxametallacycle (OMC) which requires an oxygen vacancy to form. It has been proposed that the OMC intermediate can form either EO or acetaldehyde (AA) which in turn is rapidly oxidized to CO_2 on Ag [12].

Most of the previous conclusions were mainly based on studies under ultra-high vacuum conditions (UHV) on clean surfaces where the state of the silver surface does not represent the working state of the catalytic surface under relevant practical conditions of temperature, pressure, and surface coverage [45]. In the presence of oxygen, silver undergoes oxygen-induced reconstruction forming a surface oxide like structure [46,47], in which silver is partially oxidized and penetrated with dissolved oxygen in the subsurface and bulk regions [48–50]. Based on DFT calculations, Van Santen et al. proposed a direct epoxidation path when the catalyst operates at conditions of high oxygen coverage. In this path, there is no need for OMC to form EO, unless an oxygen vacancy exists [44,50]. Classical experimental kinetic studies by Harriot et al. postulated that oxygen can be adsorbed on a silver oxide-like surface [51,52]. This was attempted to explain the larger than unity reaction rate order dependence in oxygen at high partial pressures of oxygen. Further microkinetic modelling by Stegelmann et al. proposed that consecutively adsorbed oxygen on top of a pre-chemisorbed O_α (most likely O_{nuc}) on a Ag surface is an O_{elec}, which forms a molecular oxygen-like structure labelled O/O*, where * is an oxygen vacancy site (i.e., bare Ag metallic site) [53]. Recent DFT coupled with in situ Raman spectroscopic studies reported the presence of complex oxygen molecular-silver structures [54,55] during ethylene epoxidation [56].

In this work, we prepared a series of unpromoted Ag/α-Al_2O_3 catalysts with average Ag particle size varying from ~20 to around 170 nm while using an intermediate surface area α-Al_2O_3 (~8 m^2/g) support which has been shown recently to minimize silver sintering [57]. In this work, we will show that for Ag particles up to 50 nm, the weight normalized reaction rate decreased, and above 50 nm it remained nearly constant. In the case of the apparent TOF, it increased with Ag particle size over the studied particle size range (~20–170 nm). These rate trends suggested an indirect contribution of Ag particle bulk structure in the reaction. It will also be shown that EO selectivity (extrapolated to zero residence time from experiments at different space velocities) was almost independent of Ag particle size. H_2-TPR before and after the reaction qualitatively supported previous proposals of larger oxygen uptake in highly polycrystalline and large Ag particle sizes (>100 nm). In situ Raman spectroscopy during ethylene epoxidation on different silver particle sizes evidenced the presence of molecular oxygen species (Raman band at ~880 cm^{-1}) for particles >100 nm most likely stabilized by subsurface oxygen (supported by H_2-TPR observations), and which are believed to be intermediate reaction species. Together, all these results support the hypothesis that increasing the Ag particle size increases the amounts of subsurface oxygen which leads to a higher concentration of reactive oxygen species.

2. Experimental

2.1. Silver precursor

Silver oxalate preparation steps were followed as reported in the literature [7,27,58,59]. Briefly, silver oxalate was prepared by mixing 0.4 M silver nitrate ($AgNO_3$, ACS, 99.9+% metal basis, Alfa Aesar 11414) aqueous solution (HPLC, Fisher Chemical, P/N W5-4) and a 0.2 M oxalic acid (Oxalic acid, 98%, anhydrous, Acros Organics, AC186432500) aqueous solution. A molar ratio of Ag

nitrate to oxalic acid of 1:2 was chosen such that the concentration of oxalate ions $C_2O_4^{2-}$ is four times that of Ag^+ ions to ensure complete consumption of the latter [60,61]. The following is an example of the preparation of a silver oxalate batch. Approximately 5 g of $AgNO_3$ were dissolved in 74 cm^3 of HPLC water in a 250 cm^3 beaker and 5.4 g of $H_2C_2O_4$ were dissolved in 294 cm^3 of HPLC water in a 1000 cm^3 beaker. The $AgNO_3$ solution was added dropwise to the $H_2C_2O_4$ solution at 60 ℃ for 20 min under stirring using a magnetic stirrer (MS-H-Pro Plus hotplate-stirrer, Scilogex). A white precipitate was immediately formed. After the addition, the $Ag_2C_2O_4$ precipitate was separated by vacuum filtration [62] (Buchi V-700) using a filter paper (Whatman, 11 μm, WHA1001325) placed in a funnel/vacuum flask system. Silver oxalate is insoluble in water; hence, deionized water (2000 cm^3) was used for several washing times during vacuum filtration to remove excess ions and possible impurities. The filtered $Ag_2C_2O_4$ was dried in a vacuum oven (Thermo Scientific, 3608-1CE) at 15 kPa and 60 ℃ overnight to avoid the risk of explosion of $Ag_2C_2O_4$ [63]. After that, the sample was stored at room temperature in amber vials (dark vial) to avoid possible decomposition by light exposure [59].

2.2. Catalyst preparation

Incipient wetness impregnation of a dried α-Al_2O_3 with a $Ag_2C_2O_4$-EDA complex was carried out at room temperature. The impregnation solution is composed of $Ag_2C_2O_4$ dissolved in EDA (ethylenediamine, >99.5%, Sigma-Aldrich, 03550) diluted with HPLC water with a fixed molar ratio of 1:4.8:16 mol ($Ag_2C_2O_4$:EDA:H_2O) for all prepared catalysts [27]. In a typical preparation of a batch of impregnation solution, 3.9 g (4.3 cm^3) of EDA was added to 3.8 g of HPLC (Fisher Chemical, P/N W5-4) water in a 20 cm^3 amber vial, after which 4 g of the prepared $Ag_2C_2O_4$ fine white powder was added to the EDA-water solution and mixed by sonication for 10 min at room temperature. The formed single phase complex solution (nearly transparent) was stored at about 4 °C in amber vials (to avoid silver reduction) and prepared freshly before each impregnation use [59].

Alpha-alumina (α-Al_2O_3, BET specific area of ~ 8 m^2/g, 0.25–0.45 μm meshed size, 99.95% Alpha Aesar P/N 42573) powder was dried at 150 ℃ overnight in static air in a drying oven (Thermo Scientific, Heratherm 51028112). A specific pore volume of 0.17 cm^3/g of α-Al_2O_3 (close to BET value of 0.19 cm^3/g) was estimated by incipient wetness impregnation of a known amount of α-Al_2O_3 with water. Catalysts with five different nominal metal loadings of 0.8, 3, 5, 9, and 30 Ag wt% were prepared by incipient wetness impregnation of α-Al_2O_3 with $Ag_2C_2O_4$-EDA aqueous solution. Due to the small specific pore volume, multiple impregnation-vacuum drying cycles were needed in the preparation of 9 and 30 Ag wt% catalysts, ensuring that each cycle filled the pores with a calculated overall solution volume. Once one impregnation cycle was complete by consecutive dropwise addition of silver solution and thorough mixing, the sample was dried in a vacuum oven (Thermo Scientific, 3608-1CE) at 15 kPa and 60 ℃ for 6 h, after which similar steps were repeated for the subsequent cycles. Additional details on the catalysts' preparation is provided in Section S1 and **Tables S1 and S2** in the supporting information.

The vacuum dried α-Al_2O_3 supported silver samples were then treated in a tube furnace instrument (Thermo Scientific, Thermolyne 79300) in different gas atmospheres using pure H_2 (UHP, Matheson), N_2 (UHP, Matheson), or O_2 (UHP, Matheson) under flowing conditions at 250 or 350℃ to vary the silver particle size. Gas flow into the tube furnace was adjusted using a rotameter so that a space velocity of ~600 $cm^3\ g_{cat}^{-1}\ min^{-1}$ is maintained. Under a certain gas atmosphere, the samples were heated from ambient temperature to 110 ℃ (5 ℃ min^{-1}) and dwelled for 30 min, and then ramped to 250 or 350 ℃ (5 ℃ min^{-1}) and kept at that temperature for 2 h after which the sample was cooled down and stored before characterization and catalytic performance testing [27].

2.3. Characterization

2.3.1. Thermal stability and composition

Thermogravimetric analysis (TGA) was used to determine the weight loss and $Ag_2C_2O_4$-EDA complex decomposition temperature of the different impregnated but only vacuum dried $Ag_2C_2O_4$-EDA/α-Al_2O_3 catalyst samples (~80–100 mg). The experiment was conducted in oxidative atmosphere (air) and inert atmosphere (N_2) with 100 $cm^3\ min^{-1}$ from ambient temperature up to 500 ℃ at a temperature ramp of 5 ℃ min^{-1}.

2.3.2. Morphology

X-ray diffraction (XRD) was carried out with a PANalytical Empyrean diffractometer equipped with Cu Kα radiation (45 kV, 40 mA, λ = 0.154 nm) which was used to obtain the crystalline phases present in the samples treated at high temperatures over the 2θ range of 5-80°. The crystallite size was estimated by the Scherrer equation [64]: $d_{crystallite} = \frac{K\lambda}{\beta \cos\theta}$, where K, λ, and θ are the Scherrer constant (0.9 assuming spherical crystallites), 0.154 nm (Cu), and the Bragg angle (in degrees), respectively. The full-width-at-half-maximum β (in radians) was estimated using the full width at half maximum (FWMH) and checked by calculating the integral breadth [65]. The peaks were fitted using a Pseudo-Voigt function (Gauss and Lorentz functions).

Surface morphology and local elemental mapping were determined by scanning electron microscopy (SEM, Versa 3D dual beam SEM/Focused Ion Beam) and energy-dispersive X-ray spectroscopy (EDX, Oxford). ImageJ software was used to count 100–150 silver particles on at least three different regions by assuming spherical silver particles. The average Ag particle size d_{SEM} (with standard deviation σ_{SEM}) is calculated using Eq. (1).

$$d_{SEM} \pm \sigma_{SEM} = \frac{\sum_{i=1}^{n} d_i}{n} \pm \sqrt{\frac{1}{n}\sum_{i=1}^{n}(d_{SEM} - d_i)} \quad (1)$$

where n and d_i are the number of the counted particles and the diameter of a single particle *i*, respectively. The theoretical interparticle distance (IPD) is defined as the edge-to-edge distance among neighboring spherical Ag particles assuming particles that are equally distanced to surrounding ones in a hexagonal arrangement (resembling a quasi-close packing) as calculated by Eq. (2) [66].

$$IPD = \sqrt{\frac{A}{N}} - d_{SEM} \quad (2)$$

where A and N are the BET specific surface area of the support and the number of Ag particles per gram of catalyst, respectively. N is calculated from the amount of Ag loaded on the support. As an approximation, particles are assumed to be spherical and monodispersed. Additionally, elemental compositions were determined by X-ray fluorescence (XRF) using a PANalytical Zetium instrument. Typical SEM images, silver particle size distributions, and elemental mapping results for the prepared catalysts are shown in **Figs. S1–S7**.

Nitrogen adsorption–desorption isotherms were measured at −196 ℃ using an Autosorb-iQ2 analyzer (Quantachrome Instruments). Prior to physisorption, about 1 g of α-Al_2O_3 was loaded in a 9 mm wide sample cell (P/N 74200-9L, Quantachrome Instruments) and heated in vacuum at 300 ℃ for 3 h at a rate of 5 ℃ min^{-1}. After degassing, the analysis was carried out with a standard method consisting of 21 adsorption points and 20 desorption points. The resulting BET surface area, pore volume, and average pore diameter were 7.5 $m^2\ g^{-1}$, 0.19 $cm^3\ g^{-1}$, and 105 nm, respectively.

2.4. Catalytic testing

Ethylene epoxidation over the prepared Ag/α-Al_2O_3 catalysts was carried out in a fixed bed reactor (1/2″ OD, 0.444″ ID, 427 mm long) made of stainless steel (SS304) mounted vertically. A quartz liner tube (8 mm ID × 10 mm OD, 430 mm long, Technical Glass Products) was inserted in the reactor to avoid possible reactions on the reactor wall. Coarse quartz wool (CQ-wool-0.5, Technical Glass Products) was used to hold the powdered catalyst in the middle of the reactor. The fixed bed reactor is also equipped with a tube furnace (EQ-OTF1200X-S-H-110 V, MTI Corp.) and a temperature controller (GSL-1100X-NT-110-LD, MTI Corp.). The fixed bed temperature was measured by a thermocouple placed in the middle of the catalyst sample.

Samples of freshly prepared powdered catalysts crushed and sieved to a catalyst particle size range of 20–38 μm were used. Approximately 5–20 mg of catalyst was loaded in the fixed bed reactor and interparticle-diluted with silica sand (silicon dioxide, Sigma-Aldrich, BCBV1579, crushed to 20–38 μm and pre-calcined at 600 ℃) on a weight basis ratio of catalyst/SiO_2 = 1/10. The diluted catalyst sample was initially heated to 50 ℃ and flushed with Ar. The cell was then heated to 200 ℃ at a 10 ℃/min heating rate in Ar then pretreated with 5% O_2/Ar at 200 ℃ and space velocity of 1500 $cm^3 g_{cat}^{-1} min^{-1}$ (gas flow rate per gram of active catalyst) and dwelled for 2 h. The reaction mixture composed of 10% C_2H_4, 5% O_2 balanced with Ar was introduced and the space velocity (based on total gas flow rate and undiluted catalyst) was varied between 3000 and 18,000 $cm^3 g_{cat}^{-1} min^{-1}$. These conditions ensured operation outside the mixture explosive region [67] and operation as a differential reactor. In a typical run, after achieving steady state operation, four different space velocities were tested to assess the absence of mass transport limitations. The absence of catalyst deactivation was also verified for each catalyst by retesting the initial space velocity at the end of the experimental series. Unreacted ethylene and products were quantified over 1 h of reaction at each space velocity by an online SRI 8610C GC equipped with an Rt-Q-BOND PLOT column (30 m × 0.53 mm, 20 μm, P/N 19742–6850, RESTEK), a methanizer, and a flame ionization detector (FID). The outlet gas stream was also monitored online by mass spectrometry (OmniStar GSD 320O Mass spectrometer, Pfeiffer).

Ethylene conversion (X_E) and ethylene oxide selectivity (S_{EO}) were calculated as described in the supporting information (Section S2). Two parameters were used for catalytic activity assessment: (1) Quasi steady-state ethylene consumption rate normalized by total Ag weight (m_{Ag}) given by:

$$R_E(mol_{Ethylene}\, g_{Ag}^{-1}\, s^{-1}) = \frac{X_E\, F_{E,in}}{m_{Ag}} \quad (3)$$

where $F_{E,in}$ is the inlet ethylene molar flowrates (mol s^{-1}) and (2) Apparent turnover frequency (TOF) defined as the moles of ethylene reacted per surface Ag moles (n_{Ag}) per second as determined by:

$$TOF\,(s^{-1}) = \frac{X_E\, F_{E,in}}{n_{Ag} D} \quad (4)$$

where D is the Ag metal dispersion (i.e., surface Ag atoms divided by total Ag atoms in a Ag nanoparticle). Here, for simplicity Ag particles are assumed to be semi-spherical, leading to the approximate relationship between dispersion D and average SEM Ag particle size (d_{SEM}) given by [67]:

$$D(nm) \approx \frac{1.34}{d_{SEM}} \quad (5)$$

It is important to note that the "apparent TOF" term is used here because of the ambiguity about the true nature and density of the catalyst active sites. However, as an initial approach it is deemed acceptable to determine the activity per exposed (surface) Ag sites. Therefore, for the purposes of catalyst comparison all silver surface atoms are roughly assumed to be active [57].

2.5. In situ Raman spectroscopy

In situ Raman spectroscopy experiments were conducted in Harrick's in situ high-temperature Raman reaction cell (HVC-MRA-5) shown in Fig. 1, which was equipped with a temperature controller (ATK-024–3, Harrick), and gas delivery system. The reaction cell has two thermocouples to monitor the cartridge heater and catalyst sample temperatures following a previously reported configuration [68]. The exit line from the cell is heated to ~100 ℃ to avoid product condensation on the tubing walls. The outlet gas stream was monitored online by mass spectrometry. A bypass line is present to verify the steady mixing of reactants prior to flow through the reaction cell. Quantification of reactants and products by MS is not reported here due to possible issues with overlapping m/z signals which may lead to underestimation of selectivities [69]. A detailed schematic of the experimental set up is provided in Section S3 in the supporting information (**Fig. S9**).

Freshly prepared catalyst samples were crushed and sieved to 38–75 μm particle size range and loaded (~0.10–0.11 g) to the reaction cell sample cup. The catalyst samples were pretreated in similar manner to those in the fixed bed reactor activity studies: (1) initially heated to 50 ℃ and flushed with Ar; (2) heated to 200 ℃ at a 10 ℃ min^{-1} heating rate in Ar; (3) pretreated with 5% O_2/Ar (300 $cm^3 g_{cat}^{-1} min^{-1}$) at 200 ℃ for 2 h and then (4) flushed with Ar. The sample was kept at 200 ℃ and a reaction mixture (300 $cm^3 g_{cat}^{-1} min^{-1}$) of 10% C_2H_4, 5% O_2 balanced with Ar was introduced at a total pressure of 1 atm. The reaction products were monitored by following their major m/z fragments (CO_2, H_2O, EO were tracked by MS using fragments m/z = 44, 18 and 29).

In situ Raman spectroscopy was performed on Ag/α-Al_2O_3 catalysts at various reaction conditions using a dispersive Raman spectrometer equipped with a confocal microscope (SENTERRA, Bruker). All spectra were collected using a green laser (532 nm wavelength) at a relatively low power of 2 mW (to minimize

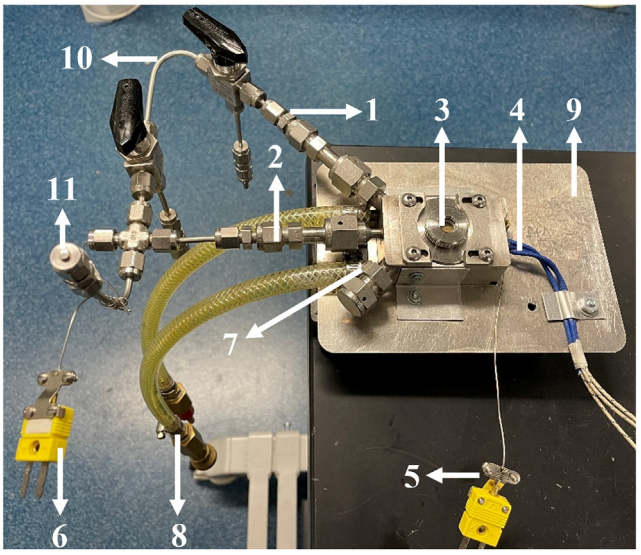

Fig. 1. Harrick Scientific in situ high-temperature Raman reaction cell. (1) gas inlet; (2) gas outlet; (3) Raman dome assembly with fused silica window (HVC-MRA); (4) cartridge heater; (5) cartridge heater/cell body thermocouple; (6) sample thermocouple via outlet line; (7) cooling ports; (8) cooling hose lines; (9) homemade cell base adapter for Bruker Senterra Raman spectrometer; (10) bypass line; (11) backflushing and cleaning line.

sample damage) and an objective lens of 50X and aperture of 1000 µm. Bruker's OPUS software was used to obtain spectra over 30 s with 20 co-additions for one measurement. Raman spectra were taken at the following conditions: (1) fresh sample at 50 ℃ in 100% Ar; (2) after oxygen pretreatment at 200 ℃ in 100% Ar; and (3) during steady state ethylene oxidation at 200 ℃ in 10% C_2H_4 and 5% O_2 after 1, 2, 3 and 4 h of reaction.

2.6. Hydrogen-temperature programmed reduction (H_2-TPR)

Temperature p... ried out in the in... (1) after oxygen ... epoxidation condi... measurement. Aft... sample temperatu... nal stabilization, H... Ar mixture (300 cr... temperature to 45...

3. Results and dis...

3.1. Ag metal loadi...

The decomposi... atmospheres is d... tion S5.1). As prev... employed pure hy... to obtain small, r... tively. Therefore, ... above the decomp... plex and of ethyle... sent work) to provide catalyst samples with different silver particle sizes and over a wide range.

In this work, the parameters used for Ag particle size control were Ag loading, treatment temperature, and the nature of the gas atmosphere. Table 1 presents the average Ag particle diameter as measured by SEM (d_{SEM}) as well as the estimated interparticle distance for all the different Ag catalysts treated at 250 and 350 ℃. The catalysts notation in this work is usually given by "Ag(nominal wt%)_SEM average diameter" or "Ag(nominal wt%)_Treatment-temperature_Gas" when comparing preparation conditions. For the latter nomenclature, the complete sample labels, preparation conditions, and Ag particle sizes are also listed in Table 1. The average Ag particle sizes ranged from 20 to 170 nm. The choice of α-Al_2O_3 with a relatively higher specific surface area (~8 m^2/g) than the industrial alumina support also allowed more control on the Ag particle size and interparticle distance (while minimizing particle size metal sintering at the relatively low reaction temperature of 200 °C).

Fig. 2 compares the obtained average silver particle sizes with the different treatment conditions. Catalysts Ag(3) and Ag(9) were both treated with N_2 and show a slight increase in the average SEM Ag particle size with increasing temperature. The higher Ag(9)

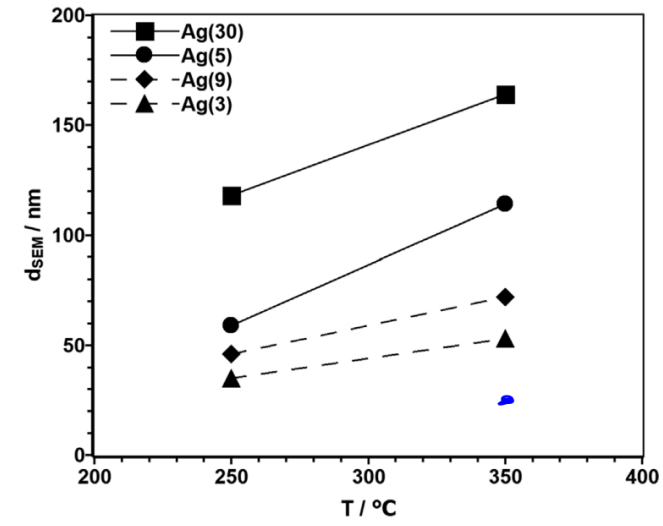

Fig. 2. Catalysts average SEM Ag particle diameter as a function of temperature and gas atmosphere (solid line: O_2 and dashed lines: N_2) after treatment for 2 h with a space velocity of 600 $cm^3\ g_{cat}^{-1}\ min^{-1}$. Trend lines added to guide the eye.

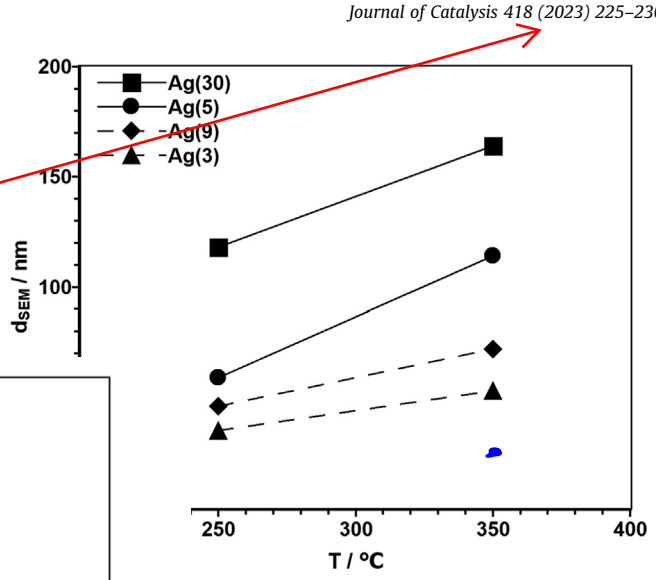

SEM Ag particle diameter as a function of temperature and ...e: O_2 and dashed lines: N_2) after treatment for 2 h with a ...^{3} g_{cat}^{-1} min^{-1}. Trend lines added to guide the eye.

...t to Ag(3) led to slightly larger Ag particle sizes ...ner silver loadings (Table 1). On the other hand, Ag(30), which were treated in O_2 resulted in a ...the average Ag particle diameter to nearly dou... lower temperature when the temperature ...0 to 350 ℃. This observation has also been ...h et al. [57] and it was attributed to the forma... ...de nanoparticles, which are mobile species that ...while decomposing to Ag metal [27], particu... ...eatments in oxidative environments [57]. Alternatively, higher Ag loadings inherently facilitate sintering which lead to particle growth and an increase in the interparticle distance.

Selected SEM images and histograms of the silver catalysts are presented in Fig. 3, whereas other images and associated elemental mapping can be found in the supporting information (**Figs. S1–S5**). All catalysts had Ag particles that were quasi spherical, except for the for Ag(30)_120 whose particles lost some of the sphericity due to sintering at this sample's high Ag loading [57,70]. Catalysts with similar average Ag diameter narrow distribution (except sample Ag (30)_120 in Fig. 3**d**) were typically obtained using different nominal Ag loadings, different heat treatment temperatures, and the same gas environment. Although catalysts Ag(3)_50 and Ag(9) _50 have almost the same average Ag particle diameter and similarly for Ag(5)_110 and Ag(30)_120, the observed interparticle distance in the SEM image becomes larger for lower Ag loading as expected from the estimated average IPD shown in Table 1.

3.2. Catalysts morphology

XRD results for the prepared catalysts are presented in Fig. 4. This figure shows that the intensity of Ag characteristic peaks at

Table 1
Average SEM Ag particle size (d_{SEM}) and estimated interparticle distance (IPD) for the prepared catalysts treated under different gas atmospheres at 250 and 350 ℃ (10 ℃ min^{-1}) for 2 h.

Ag(wt%)_Treatment Gas	*250 ℃*		*350 ℃*	
	$d_{SEM} \pm \sigma_{SEM}$	IPD/nm	$d_{SEM} \pm \sigma_{SEM}$	IPD/nm
Ag(0.8)_H_2	–	–	20 ± 10	205
Ag(3)_N_2	40 ± 10	180	50 ± 20	320
Ag(9)_N_2	50 ± 10	150	70 ± 20	315
Ag(5)_O_2	60 ± 40	345	110 ± 50	970
Ag(30)_O_2	120 ± 80	280	170 ± 100	500

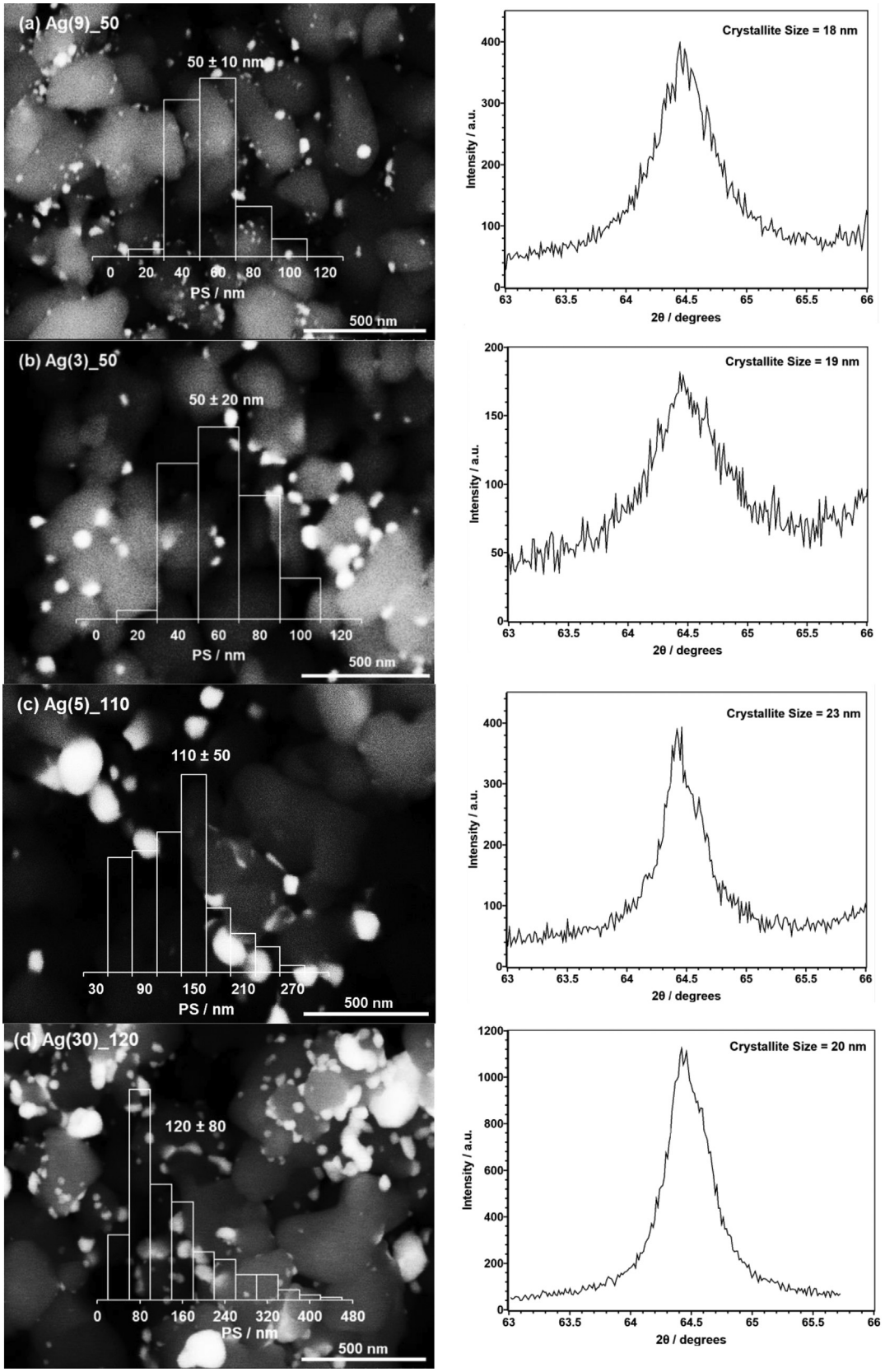

Fig. 3. SEM images, silver particle size histograms, and XRD diffractograms of the Ag(220) for (a) Ag(9)_50, (b) Ag(3)_50, (c) Ag(5)_110, and (d) Ag(30)_120.

2θ values of 38.1, 44.2, 64.5, and 77.4° increased with increasing Ag loading, reaching the highest values for Ag(30). The absence of additional peaks illustrates the appreciable decomposition of Ag organic precursor compounds by heat treatment regardless of the gas atmosphere during catalyst preparation. Ag(220) reflection was used to estimate the crystallite size as reported earlier [15].

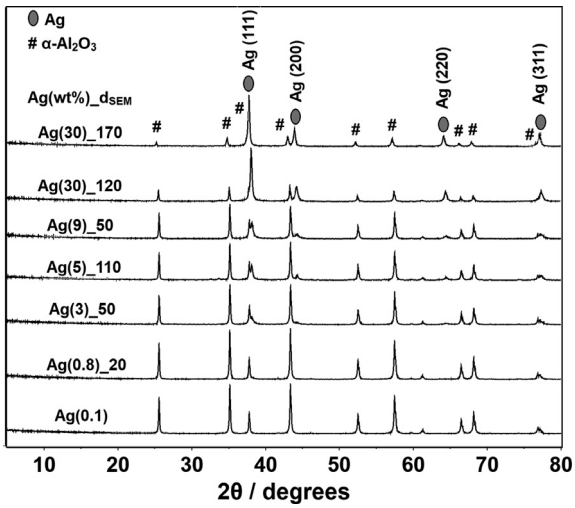

Fig. 4. XRD patterns for various Ag/α-Al_2O_3 catalysts presented in Table 2. The diffractograms are offset for clarity.

The Ag reflections for catalyst samples Ag(0.1) and Ag(0.8)_20 could not be detected, as shown in **Fig. S13** (supporting information) because of Ag low loading, high dispersion, and/or low crystallite size, which is well below the XRD instrument sensitivity limit. The SEM image of Ag(0.8)_20 and XRD patterns in **Fig. S13** clearly illustrates the high dispersity in the low Ag loading samples.

Table 2 summarizes the results for particle and crystallite sizes as determined from SEM and XRD analysis, respectively. From this table it can be noted that all crystallite sizes were found to be similar and in the range of 18–23 nm. However, the SEM average particle diameter for all studied catalysts in this table was larger than the crystallite size obtained by XRD. Similar observations have been reported and used as evidence that Ag particles consist of multiple crystallites that are separated by intergrain boundaries for average particle diameters >40 nm [15,16]. These results imply that the Ag(0.8)_20 catalyst has a homogeneous monocrystalline (i.e., one crystallite/per Ag particle) structure compared to the multicrystallite particles present in other catalysts. Based on the polycrystallinity of Ag particles, it seems like there is a dominant Ostwald growth mechanism [48,55] and a less predominant particle coalescence mechanism during catalyst preparation [42].

3.3. Catalytic activity and ethylene oxide selectivity measurements

For all catalysts tested, it was found that steady-state operation was achieved within 1 h of reaction (Section S2, **Fig. S8**). For all catalytic activity and selectivity testing, the absence of mass and heat transfer limitations was evaluated as detailed in the supporting information (Section S4). From the catalytic activity testing results at different space velocities, it was found that external mass transfer limitations, which can limit catalytic activity comparison among different catalysts, can exist even at conversions below 1%. For example, **Fig. S11** in Section S4.2 shows that the weight-normalized ethylene conversion rate increases with the square root of the ratio of volumetric flowrate to catalyst particle size indicating the presence of external diffusion limitations. It was found that ethylene conversions lower than 0.5% and space velocities higher than 6000–9000 $cm^3 g_{cat}^{-1} min^{-1}$ were required to eliminate such mass transport issues as well as to minimize possible product inhibition effects such as those previously reported for propylene epoxidation reaction [71]. These results highlight the risks of relying on only theoretical calculations for external mass transfer limitations due to the lack of reliable mass transfer coefficient correlations at the small Re and Sc numbers commonly present in laboratory reactors. For these reasons and for rigorous comparison of catalysts, catalytic activity and ethylene oxide selectivity results are reported at extrapolated residence time of zero as shown in Table 3.

Fig. 5(left) presents ethylene conversion vs EO selectivity for the tested Ag/α-Al_2O_3 catalysts. The figure shows the typical inverse relationship between conversion and selectivity for a primary product. As conversion increases, the primary product (EO) can undergo secondary reactions to form CO_2 (on Ag) and/or acetaldehyde (on α-Al_2O_3's hydroxyl groups) [50], leading to a decrease in the selectivity. Fig. 5(right) shows EO selectivity extrapolated to residence time zero (to minimize the confounding effects of conversion, inhibition, and exposed support surface) as a function of the average silver particle size. Overall, the EO selectivity is found to be nearly independent of silver particle size. These selectivity trends match previous reports by de Jongh and co-workers [27,57] and Hensen and co-workers [15].

3.4. Silver particle size effects on the rate of reaction and apparent TOF

The catalytic activity of the tested catalysts was normalized to the average exposed surface area of the silver nanoparticles. For these rates, the average Ag particle sizes of the freshly prepared catalysts (as determined by SEM) were used for simplicity since no significant changes were observed in the average Ag particle size in the used catalysts after reaction (**Figs. S6 and S7**). The stability of these catalysts to sintering was also reported earlier for a similar support specific area and reaction conditions [27,57]. Fig. 6 shows the rate of ethylene oxidation normalized by the total weight of silver and apparent TOF (moles of ethylene reacted per moles of surface Ag per second), respectively, against the average Ag particle size. For particles up to around 50 nm, the weight normalized conversion rate decreased rapidly and above ~ 50 nm the conversion rate remained nearly constant. In contrast, the apparent TOF increased with the average silver particle size. These observations are similar to those reported by Hensen and co-workers [15]. In general, silver particles of 50–70 nm or larger have been commonly reported to be more active based on apparent TOF [24,27,70,72,73].

For most structure sensitive reactions, it is commonly assumed that TOF will be higher for smaller particles showing high dispersion [70]. However, this does not seem to be the case for ethylene epoxidation (at least based on apparent TOF) for which the TOF

Table 2
XRD and SEM analysis of representative Ag/α-Al_2O_3 catalysts.

Name Ag(wt%)_ D_{SEM}	Ag Loading (wt%)	Temperature(℃)_atmosphere	d_{SEM} (nm)	d_{XRD} (nm)
Ag(30)_170	29.6	350_O_2	170	23
Ag(30)_120	29.6	250_O_2	120	20
Ag(9)_50	9.2	250_N_2	50	18
Ag(5)_110	4.9	350_O_2	110	23
Ag(3)_50	3.7	350_N_2	50	19
Ag(0.8)_20	0.8	350_H_2	20	–

Table 3
Summary of Ag/α-Al_2O_3 catalysts preparation conditions, structure properties, and catalytic performance results extrapolated to zero residence time.

	Catalyst Notation (Ag(wt%)_ d_{SEM})					
	Ag(0.8)_20	Ag(9)_50	Ag(3)_50	Ag(5)_110	Ag(30)_120	Ag (30)_170
Preparation T (°C)	350	250	350	350	250	350
Preparation gas	H_2	N_2	N_2	O_2	O_2	O_2
d_{SEM} (nm) ± σ_{SEM}	20 ± 10	50 ± 10	50 ± 20	110 ± 50	120 ± 80	170 ± 100
IPD (nm)	205	150	320	970	280	500
EO Selectivity (%)	49	59	52	57	60	57
R_E*	2.6	1.4	1.6	0.9	1.3	0.8
Apparent TOF (s^{-1})**	4.5	5.3	6.4	8.5	12.4	10.6

* Weight-normalized ethylene conversion rate extrapolated to residence time zero (mol g_{Ag}^{-1} s^{-1} × 10^{-7}) ** Moles of ethylene reacted per surface Ag moles per second × 10^{-4}
Reaction conditions: 200 °C, 1 atm, 10% C_2H_4, 5% O_2.

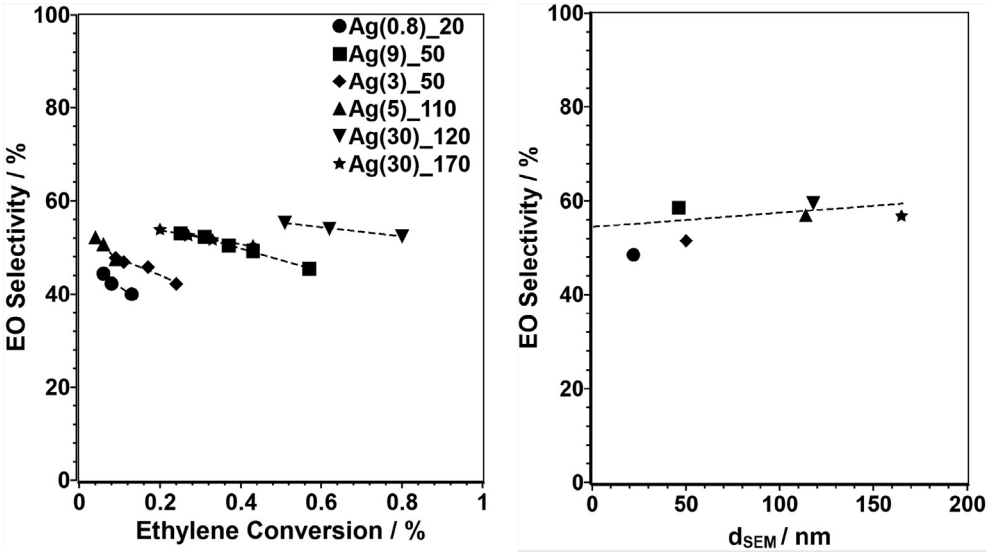

Fig. 5. (Left) Ethylene conversion vs EO selectivity obtained at different space velocities (~6000–18000 cm^3 g_{cat}^{-1} min^{-1}) and (Right) Ag particle size vs EO selectivity (extrapolated to zero residence time) for the prepared Ag/α-Al_2O_3 catalysts. Reaction conditions: 200 °C, 1 atm, 10% C_2H_4, 5% O_2, lines were added to guide the eye.

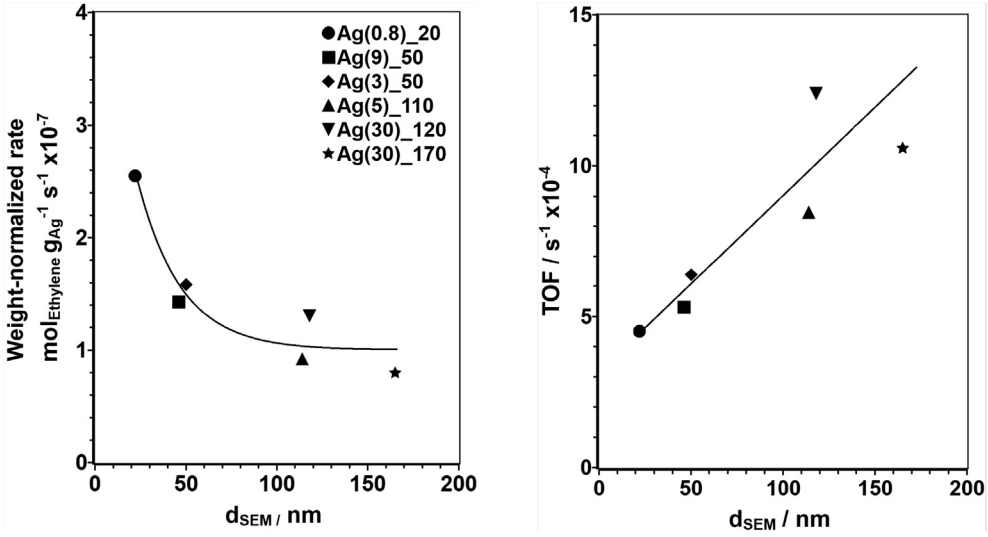

Fig. 6. (Left) Weight-normalized ethylene conversion rate as a function of the Ag particle size and (Right) apparent TOF (moles of ethylene converted per moles of surface Ag per second) as a function of the Ag particle size (extrapolated to zero residence time) for the prepared Ag/α-Al_2O_3 catalysts. Reaction conditions: 200 °C, 1 atm, 10% C_2H_4, 5% O_2. Solid lines were added to guide the eye.

increases with Ag particle size, leading investigators to study other factors such as the bulk structure of such relatively large particles [15,16,72,73]. The effect of Ag particle size on apparent TOF (Fig. 6) resembles an atypical (antipathetic) particle size-TOF relationship, also known as negative particle size effect, demonstrating the unusual role of Ag surface area for catalyzing the reaction in which large Ag particles have high catalytic activity. This increase in apparent TOF with larger Ag particle sizes defies expectations of

low TOF for larger metal particle sizes since the reaction rate scales typically with surface area in more common sympathetic structure-sensitive reactions. At present, the reasons for this behavior are unknown, but the lack of knowledge on the true nature of active sites and their counting probably contribute to the current unusual observations based on apparent TOFs. Other than particle size and the corresponding silver exposed surface area, silver particles also differ in their bulk structure as shown by XRD and SEM where Ag particles most likely consists of multiple crystallites which increase proportionally with increases in particle size (Section S5.3, **Fig. S14**). It is unclear if these differences are related to the unusual behavior of silver catalysts for EO synthesis, but this has led to speculations that Ag particle bulk structure plays an essential role in the reaction, manifested in the observed structure sensitivity of the ethylene epoxidation reaction.

In general, quasi spherical silver particles with fcc structure have predominantly regular Ag surfaces Ag(1 1 1), which is the most stable facet for large particles [74]. As noted above, the apparent TOF behavior with such large particles (>20 nm) is unusual because they are expected to resemble more closely the bulk metal on which the emergence of active sites due to structural variation no longer occurs [10,11]. If the polycrystallinity of large silver particles is of relevance for ethylene epoxidation, then this may be due to the presence of defects at the grain boundaries that separate the crystallites. Such defects have been postulated to enhance oxygen diffusion to silver bulk [75,76]. To explain the increase in the apparent TOF with Ag particle size, Hensen and co-workers proposed that oxygen is activated on the defects near the grain boundaries where oxygen in the metal bulk diffuses to subsurface regions and eventually to the external surface to react with ethylene [15]. While plausible, many questions remain with this proposal. For example, it is unclear if atomic oxygen will diffuse out of silver bulk and participate in the oxidation reaction, in particular, at high oxygen partial pressures (20 bar) such as those previously reported [15]. An alternative explanation is the relevance of subsurface oxygen for the formation of reactive oxygen species [6,30], which seems to agree with the increase of apparent TOF with Ag particle size based on the following observation: that the oxygen content remaining in large Ag particles (>100 nm) is relatively larger than those in smaller ones (<100 nm) as assessed by comparing H_2-TPR before and after the reaction for all catalysts (see Section S5.5 and **Fig. S16**). This relatively higher overall oxygen content is presumed to affect the stability of reactive oxygen species. The possible presence of different surface oxygen species is explored next by in situ Raman spectroscopy at ethylene epoxidation conditions.

3.5. In situ Raman spectroscopy at ethylene epoxidation reaction conditions

In this section, in situ Raman spectra after oxygen pretreatment and during ethylene epoxidation reaction will be presented for catalysts with Ag particle sizes of 20, 50, 120 and 170 nm. In situ Raman spectra were taken after oxygen pretreatment at 200 ℃ and during reaction (10% C_2H_4, 5% O_2) at 1 atm and 200 ℃ for 4 h (steady state operation was achieved after ~ 1–2 h, **Fig. S15**). A review of previously reported Raman bands during silver exposure to oxygen, ethylene, and/or reaction mixture and their assignments is shown in **Table S4.** Table 4 below summarizes the most relevant Raman bands to this work detected during in situ measurements. Fig. 7 presents the in situ Raman spectra for Ag/α-Al_2O_3 catalysts with average Ag particle sizes of 20, 50, 120 and 170 nm (additional Raman spectra for fresh catalysts and for Ag (3)_50 nm are shown in **Figs. S17 and S18** in Section S6).

The band at 580 cm^{-1} appeared after the oxygen pretreatment for all catalysts and is particularly intensified for particles >100 nm. The shoulder at 680 cm^{-1} also appeared after the pretreatment, and its intensity was appreciable in the case of the 170 nm Ag particle size catalyst sample, but barely noticeable for other particle sizes. The in situ Raman spectra (**Figs. 7 and S18**) shows the intensification of bands 399 and 440 cm^{-1} and emergence of features between ~800 and 1000 during ethylene epoxidation reaction demonstrating that Ag catalysts becomes oxidized when exposed to rection conditions, as reported earlier [56]**.** The intensity of the band at 399 cm^{-1} increased slightly during ethylene epoxidation reaction for all catalysts. The intensity of the band at 440 cm^{-1} remained unchanged for particles <100 nm but slowly intensified for larger particles. A small peak emerged for all samples at 815 cm^{-1} during ethylene epoxidation reaction. This band at 815 cm^{-1} attenuated for particles >100 nm and it correlated with the intensification of a characteristic feature at 880 cm^{-1} for catalysts Ag(30)_120 and Ag(30)_170 as a function of reaction time. For the Ag(30)_170 catalyst, in situ Raman spectra acquired after 10 min of reaction confirmed the emergence of the 880 cm^{-1} feature due to ethylene epoxidation. Other Raman features emerged during reaction at 1040 and 1080 cm^{-1} and grew with reaction time for all samples.

The Raman assignments of relevant features in this work which are summarized in Table 4 are supported by recent DFT guided studies. The band at 399 cm^{-1} is generally assigned to Ag-O vibrations as frequently reported in the literature (**Table S4).** As discussed above, H_2-TPR after reaction (**Fig S16**) showed that polycrystalline particles >100 nm have relative larger hydrogen consumption. Therefore, the band at 440 cm^{-1} is assigned to bulk oxygen as reported by Wachs and co-workers [56]. The band at 580 cm^{-1} was assigned to O-Ag-O motifs vibrations as suggested by Paolucci and co-workers's for multiple Ag_2O structures and ascribed to O-Ag-O motifs that can be a combination of surface and subsurface oxygens. Further support for this assignment comes from an earlier observation of a 545 cm^{-1} band attenuation during the thermal decomposition of silver oxide [79]. The shoulder at 680 cm^{-1} has been assigned to multiple oxygen species (Table S4). Nevertheless, the bands at 668 and 691 cm^{-1} reported

Table 4
Summary of relevant in situ Raman bands and oxygen species assignments during ethylene epoxidation on silver.*

Raman bands in this work (cm^{-1})	Species	Literature reports (cm^{-1})
399	ν(Ag-O) on Ag Surface	399 [54]
		389 [56]
440	ν(O-Ag-O) in bulk Ag	449 [56]
	ν(O-Ag-O) in subsurface Ag	436 [77,78]
580	ν(O-Ag-O) in surface and subsurface oxygen motifs	500–586 [54]
680	ν(O-O) in subsurface atomic-molecular hybrid structure: Ag_2-O-O-Ag_2	668 [55]
	ν(O-O) in trough site: Ag_4-O-O structure	693 [56]
815 and 880	ν(O-O) in surface atomic-molecular hybrid structure: Ag_2-O-O-Ag_2	806 [55]
	ν(O-O) in surface Ag_4-O-O structure	839[56]
	ν(O-O) in molecular oxygen complex Ag_x.O-O stabilized by subsurface atomic oxygen	810–840 [54]

* Most Raman band assignments supported by DFT calculations are listed here. A more comprehensive literature review of band assignments is shown in **Table S4**.

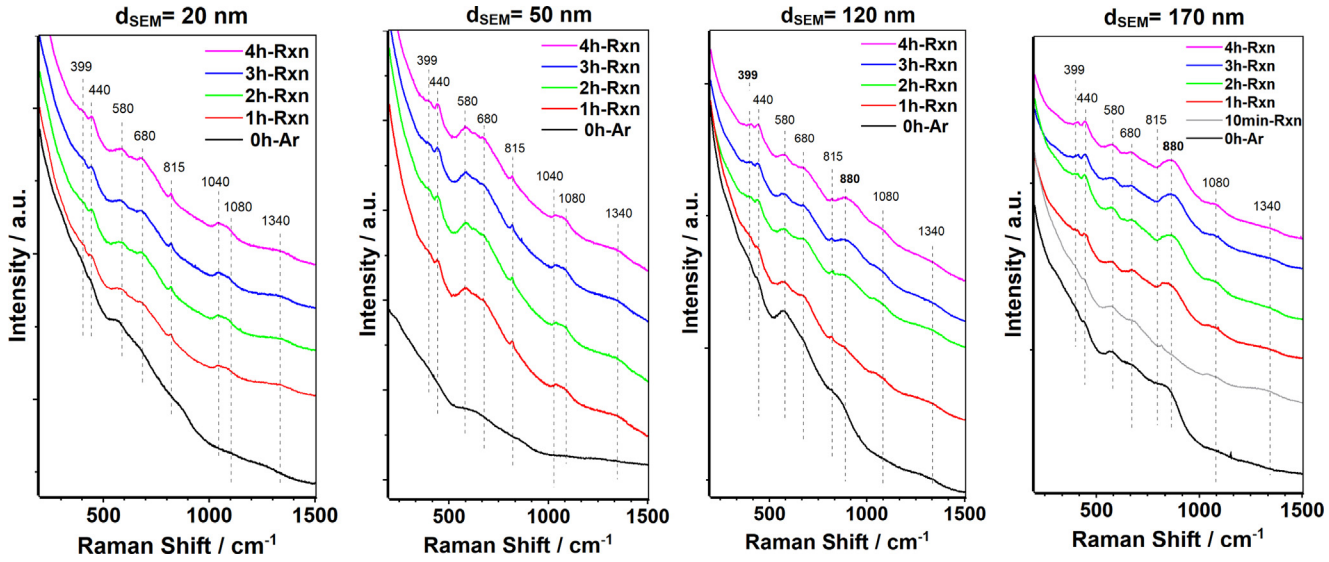

Fig. 7. In situ Raman spectra after O_2 pretreatment in Ar flow (black: before reactants exposure) and ethylene epoxidation after 1 (red), 2 (green), 3 (blue), and 4 h (magenta) on unpromoted Ag/α-Al_2O_3 catalysts (from left to right): Ag(0.8)__20, Ag(9)_50, Ag(30)_120 and Ag(30)_170. Various surface and subsurface species formed on supported Ag following contact with the reactant mixture of 10% C_2H_4 and 5% O_2 for ethylene epoxidation at 200 °C and 1 atm. Spectra acquired with 532 nm laser wavelength, 2 mW power. (For interpretation of the references to colour in this figure legend, the reader is referred to the web version of this article.)

by Podkolzin and co-workers and Wachs and co-workers, respectively, suggested that they could be due to a subsurface atomic-molecular oxygen hybrid structure [55,56] (Ag_2-O-O-Ag_2 is similar to Ag_4-O-O in Table 4); however, contributions to this band from adsorbed carbonates cannot be excluded.

The emergence of features at 815 and 880 cm^{-1} during the reaction indicates that they may be due to intermediate species contributing to the reaction. The band near ~800 cm^{-1} was suggested to represent reactive atomic oxygen species in ethylene epoxidation [80] and previous DFT calculations assigned it to an interaction between surface and subsurface oxygen atoms O_α–O_γ on partially oxidized Ag [6,81]. However, during reaction conditions, Wachs and coworkers investigated p(4 × 4) – O/Ag(1 1 1) with quasi in situ HS-LEIS, in situ NAP-XPS, and in situ Raman spectroscopy after an oxidation treatment and during ethylene oxidation, and provided compelling evidence that the surface molecular oxygen structure Ag_4–O_2 (near 800 cm^{-1}) is an active oxygen species for ethylene epoxidation [56]. This species is similar to the surface atomic-molecular hybrid structure Ag_2-O-O-Ag_2 previously reported by Podkolzin and co-workers. This hybrid oxygen species required dissociation of molecular oxygen but still possess the O-O bond because one of the adsorbed O atom reacts with one lattice O atom on the surface or subsurface of Ag. More importantly, these hybrid oxygen structures were described as a metastable species that can be catalytically active in selective oxidation reactions on Ag catalysts [55].

Raman features in the range of 1040–1080 cm^1 are tentatively assigned to O-O vibrations in absorbed molecular oxygen and/or surface monodentate and bidentate carbonates adsorbed on Ag as shown in Table S4. In our work, these peaks did not appear for the fresh catalysts (**Fig. S17**), nor after O_2 pretreatment (Fig. 7) and only appeared during ethylene epoxidation reaction. It is unlikely that these Raman bands are due to the presence of carbonates of alkali metal (e.g., Na, K) impurities (which could affect catalytic activity and selectivity) since they were not detected by in situ Raman during exposure of the support to CO_2 at 200 °C (Section S6.3, **Fig. S19**) neither (at instrument's sensitivity levels) by XPS and EDX elemental mapping of the silver catalysts (Section S6.4, **Fig. S20**).

The key new feature from the current in situ Raman studies during ethylene epoxidation reaction is the band around 880 cm^{-1} that evolved significantly for Ag particle sizes >100 nm and grew during reaction. Paolucci and co-workers conducted an in situ Raman spectroscopy study of unsupported silver nanoparticles (80–100 nm) under ethylene epoxidation conditions with complementary computed Raman frequencies using DFT calculations for several Ag_xO_y reconstructed surfaces [54]. They reported a band centered between 810 and 840 cm^{-1} and provided evidence for bands in the range of 800–1000 cm^{-1} as being due to molecular oxygen complexes stabilized by surface and/or subsurface atomic oxygen. Therefore, the band at 880 cm^{-1} is ascribed to a stabilized molecular oxygen complex structure. The stabilizing agent is a neighbouring atomic oxygen species that is speculated to be a subsurface or bulk oxygen represented by the observed Raman band at 440 cm^{-1} [56]. For particles >100 nm, after the oxygen pretreatment and during the reaction, the band at 440 cm^{-1} was intensified indicating the formation of substantial amounts subsurface/bulk oxygen species during the oxygen pretreatment. This subsurface oxygen appears to play an important role in the stabilization of reactive oxygen species and it has been reported to be highly stable at reaction temperature [77,78]. Also, it has been reported that subsurface oxygen is required to form electrophilic active oxygen species on silver [29,37,82]. Overall, it is possible that the higher degree of polycrystallinity in catalyst samples with large Ag particle sizes may facilitate oxygen uptake as suggested [15,16] by SEM, XRD and H_2-TPR after reaction; however, additional systematic in situ studies are required to establish such correlation between silver particle structure and catalytic activity and selectivity.

Regardless of the assignment of the band at 880 cm^{-1}, particles >100 nm are most likely to have significant larger amounts of oxygen species represented by this band. In addition to active oxygen species represented by 815 cm^{-1} that appeared for all catalysts, the appearance of the oxygen species at 880 cm^{-1} for catalysts with Ag particle size >100 nm implies an increase in the number of active oxygen species resulting in an enhanced apparent TOF. The observed variations of in situ Raman bands with silver particle size in unpromoted Ag/α-Al_2O_3 catalysts provide further spectroscopic evidence of the silver particle size effect on the ethylene epoxidation activity through the formation of multiple reactive oxygen species for relatively large Ag particles (>100 nm).

4. Conclusion

In this work, the controlled synthesis of unpromoted Ag/α-Al_2O_3 was achieved by treating samples of α-Al_2O_3 support (~8 m^2/g) impregnated with a silver oxalate solution at different temperatures and under different gas atmospheres leading to Ag particle sizes between ~20 and 170 nm. Characterization by SEM and XRD showed that silver particles consist of multiple crystallites. It was found that ethylene epoxidation had an atypical TOF-particle size relationship, where the apparent TOF increased with increasing Ag particle size. The opposite relationship was observed for the weight normalized conversion rate vs Ag particle size. Meanwhile, EO selectivity (extrapolated to zero residence time) was nearly unaffected (~50–60%) by Ag particle size. In situ Raman during ethylene epoxidation on unpromoted Ag/α-Al_2O_3 with different average Ag particle sizes revealed the presence of a Raman band at 815 cm^{-1} for all catalysts, which was assigned to molecular oxygen complex species. Moreover, in situ Raman also revealed the evolution of a significant band at 880 cm^{-1} for large particles (>100 nm) attributed to molecular oxygen complex species as reported in literature and this species is presumably stabilized by subsurface oxygen as suggested from H_2-TPR results. The results of this work provide in situ Raman spectroscopic evidence for the presence of several active oxygen species during ethylene epoxidation on Ag/α-Al_2O_3 catalysts. Particularly, catalysts with larger Ag particles show two active oxygen species (characterized by Raman bands at 815 and 880 cm^{-1}), which are more likely responsible for their higher apparent TOF in ethylene epoxidation.

Data availability

Data will be made available on request.

Declaration of Competing Interest

The authors declare that they have no known competing financial interests or personal relationships that could have appeared to influence the work reported in this paper.

Acknowledgments

The authors acknowledge the financial support by the National Science Foundation under grants No CBET-1847655. H.A.A. also would like to thank the government of the Kingdom of Saudi Arabia and King Abdulaziz University for their financial support in his graduate study at the University of Kansas.

Appendix A. Supplementary material

Supplementary data to this article can be found online at https://doi.org/10.1016/j.jcat.2023.01.016.

References

[1] The Global Ethylene Oxide Market (2017-2023). <https://www.businesswire.com/news/home/20181126005406/en/The-Global-Ethylene-Oxide-Market-2017-2023—ResearchAndMarkets.com> (Accessed 01-23-2022).
[2] W.H. Faveere, S. Van Praet, B. Vermeeren, K.N.R. Dumoleijn, K. Moonen, E. Taarning, B.F. Sels, Toward replacing ethylene oxide in a sustainable world: Glycolaldehyde as a bio-based C2 platform molecule, Angew. Chem., Int. Ed. 60 (2021) 12204–12223.
[3] IHS Chemical Economics Handbook. <https://ihsmarkit.com/products/ethylene-oxide-chemical-economics-handbook.html> (Accessed 01-23-2022).
[4] S. Rebsdat, D. Mayer, Ethylene glycol, in: Ullmann's Encyclopedia of Industrial Chemistry, 2000.
[5] T.E. Lefort, Process for the production of ethylene oxide, US1998878A, 1931.
[6] T. Pu, H. Tian, M.E. Ford, S. Rangarajan, I.E. Wachs, Overview of selective oxidation of ethylene to ethylene oxide by Ag catalysts, ACS Catal. 9 (2019) 10727–10750.
[7] L.G. Pinaeva, A.S. Noskov, Prospects for the development of ethylene oxide production catalysts and processes (review), Pet. Chem. 60 (2020) 1191–1206.
[8] B. Subramaniam, R.K. Helling, C.J. Bode, Quantitative sustainability analysis: a powerful tool to develop resource-efficient catalytic technologies, ACS Sust. Chem. Eng. 4 (2016) 5859–5865.
[9] M. Lamoth, T. Jones, M. Plodinec, A. Machoke, S. Wrabetz, M. Krämer, A. Karpov, F. Rosowski, S. Piccinin, R. Schlögl, E. Frei, Nanocatalysts unravel the selective state of Ag, ChemCatChem 12 (2020) 2977–2988.
[10] R.A. van Santen, Complementary structure sensitive and insensitive catalytic relationships, Acc. Chem. Res. 42 (2009) 57–66.
[11] D.J. Sajkowski, M. Boudart, Structure sensitivity of the catalytic oxidation of ethene by silver, Catal. Rev. - Sci. Eng. 29 (1987) 325–360.
[12] V.I. Bukhtiyarov, A. Knop-Gericke, Ethylene epoxidation over silver catalysts, in: Nanostructured Catalysts: Selective Oxidations, The Royal Society of Chemistry, 2011, pp. 214–247.
[13] R. Van Hardeveld, F. Hartog, The statistics of surface atoms and surface sites on metal crystals, Surf. Sci. 15 (1969) 189–230.
[14] C.T. Campbell, The selective epoxidation of ethylene catalyzed by Ag(111): a comparison with Ag(110), J. Catal. 94 (1985) 436–444.
[15] A.J.F. van Hoof, E.A.R. Hermans, A.P. van Bavel, H. Friedrich, E.J.M. Hensen, Structure sensitivity of silver-catalyzed ethylene epoxidation, ACS Catal. 9 (2019) 9829–9839.
[16] S.V. Tsybulya, G.N. Kryukova, S.N. Goncharova, A.N. Shmakov, B.S. Balzhinimaev, Study of the real structure of silver supported catalysts of different dispersity, J. Catal. 154 (1995) 194–200.
[17] H. Pines, C.-T. Chen, Alumina: Catalyst and support. IV. aromatization and dehydroisomerization of 1,1-dimethylcyclohexane, 4,4-dimethylcyclohexene and of methylcycloheptane over chromia-alumina catalysts, J. Am. Chem. Soc. 82 (1960) 3562–3566.
[18] Z. Łodziana, J.K. Nørskov, P. Stoltze, The stability of the hydroxylated (0001) surface of α-Al2O3, J. Chem. Phys. 118 (2003) 11179–11188.
[19] G. Boskovic, M. Baerns, Catalyst deactivation, in: M. Baerns (Ed.), Basic Principles in Applied Catalysis, Springer, Berlin Heidelberg, Berlin, Heidelberg, 2004, pp. 477–503.
[20] E. Ruckenstein, S.H. Lee, The behavior of model AgAl2O3 catalysts in various chemical environments, J. Catal. 109 (1988) 100–119.
[21] A.J.F. van Hoof, R.C.J. van der Poll, H. Friedrich, E.J.M. Hensen, Dynamics of silver particles during ethylene epoxidation, Appl. Catal., B 272 (2020).
[22] L.M. Akella, H.H. Lee, Selectivity characterization of ethylene oxidation reactions: oxygen chemisorption, J. Catal. 86 (1984) 465–472.
[23] J.E. van den Reijen, W.C. Versluis, S. Kanungo, M.F. d'Angelo, K.P. de Jong, P.E. de Jongh, From qualitative to quantitative understanding of support effects on the selectivity in silver catalyzed ethylene epoxidation, Catal. Today 338 (2019) 31–39.
[24] J.K. Lee, X.E. Verykios, R. Pitchai, Support and crystallite size effects in ethylene oxidation catalysis, Appl. Catal. 50 (1989) 171–188.
[25] S. Rojluechai, S. Chavadej, J.W. Schwank, V. Meeyoo, Catalytic activity of ethylene oxidation over Au, Ag and Au–Ag catalysts: support effect, Catal. Commun. 8 (2007) 57–64.
[26] T. Shirai, J. Wang Li, C. Ishizaki, K. Ishizaki, Surface hydration states of commercial high purity α-Al2O3 powders evaluated by temperature programmed desorption mass spectrometry and diffuse reflectance infrared Fourier transform spectroscopy, Sci. Technol. Adv. Mater. 6 (2005) 123–128.
[27] J.E. van den Reijen, S. Kanungo, T.A.J. Welling, M. Versluijs-Helder, T.A. Nijhuis, K.P. de Jong, P.E. de Jongh, Preparation and particle size effects of Ag/α-Al2O3 catalysts for ethylene epoxidation, J. Catal. 356 (2017) 65–74.
[28] L. Zhong, D. Chen, S. Zafeiratos, A mini review of in situ near-ambient pressure XPS studies on non-noble, late transition metal catalysts, Catal. Sci. Technol. 9 (2019) 3851–3867.
[29] R.A. Van Santen, H.P.C.E. Kuipers, The mechanism of ethylene epoxidation, Adv. Catal. 35 (1987) 265–321.
[30] M.O. Ozbek, R.A. van Santen, The mechanism of ethylene epoxidation catalysis, Catal. Lett. 143 (2013) 131–141.
[31] P.A. Kilty, W.M.H. Sachtler, The mechanism of The selective oxidation of ethylene to ethylene oxide, Catal. Rev. - Sci. Eng. 10 (1974) 1–16.
[32] D.W. Park, G. Gau, Ethylene epoxidation on a silver catalyst: Unsteady and steady state kinetics, J. Catal. 105 (1987) 81–94.
[33] C.T. Campbell, M.T. Paffett, The interactions of O2, CO and CO2 with Ag(110), Surf. Sci. 143 (1984) 517–535.
[34] C. Backx, C.P.M. De Groot, P. Biloen, Adsorption of oxygen on Ag(110) studied by high resolution ELS and TPD, Surf. Sci. 104 (1981) 300–317.
[35] C. Backx, J. Moolhuysen, P. Geenen, R.A. van Santen, Reactivity of oxygen adsorbed on silver powder in the epoxidation of ethylene, J. Catal. 72 (1981) 364–368.
[36] R.A. van Santen, C.P.M. de Groot, The mechanism of ethylene epoxidation, J. Catal. 98 (1986) 530–539.
[37] R.B. Grant, R.M. Lambert, A single crystal study of the silver-catalysed selective oxidation and total oxidation of ethylene, J. Catal. 92 (1985) 364–375.
[38] V.I. Bukhtiyarov, I.P. Prosvirin, R.I. Kvon, Study of reactivity of oxygen states adsorbed at a silver surface towards C2H4 by XPS, TPD and TPR, Surf. Sci. 320 (1994) L47–L50.
[39] V.I. Bukhtiyarov, V.V. Kaichev, I.P. Prosvirin, Oxygen adsorption on Ag(111): X-ray photoelectron spectroscopy (XPS), angular dependent x-ray photoelectron

spectroscopy (ADXPS) and temperature-programmed desorption (TPD) studies, J. Chem. Phys. 111 (1999) 2169–2175.
[40] V.I. Bukhtiyarov, A.I. Boronin, I.P. Prosvirin, V.I. Savchenko, Stages in the modification of a silver surface for catalysis of the partial oxidation of ethylene: II. Action of the reaction medium, J. Catal. 150 (1994) 268–273.
[41] A.G.K. Boreskov, A.V. Khasin, Reaction of ethylene with oxygen adsorbed on silver: reactivity of adsorbed oxygen atoms and modifying effect of the reaction products, Dokl. Phys. Chem. Engl. 274 (1984) 1–3.
[42] M. Özbek, I. Onal, R. van Santen, Why silver is the unique catalyst for ethylene epoxidation, J. Catal. 284 (2011) 230–235.
[43] S. Linic, M.A. Barteau, Control of ethylene epoxidation selectivity by surface oxametallacycles, J. Am. Chem. Soc. 125 (2003) 4034–4035.
[44] M.O. Ozbek, I. Onal, R.A. van Santen, Effect of surface and oxygen coverage on ethylene epoxidation, Top. Catal. 55 (2012) 710–717.
[45] M. Boudart, Chemisorption during catalytic reaction on metal surfaces, J. Vac. Sci. Technol. 12 (1975) 329–332.
[46] A.J.F. van Hoof, I.A.W. Filot, H. Friedrich, E.J.M. Hensen, Reversible restructuring of silver particles during ethylene epoxidation, ACS Catal. 8 (2018) 11794–11800.
[47] A. Reicho, A. Stierle, I. Costina, H. Dosch, Stranski-Krastanov like oxide growth on Ag(111) at atmospheric oxygen pressures, Surf. Sci. 601 (2007) L19–L23.
[48] J. Derouin, R.G. Farber, S.L. Heslop, D.R. Killelea, Formation of surface oxides and Ag2O thin films with atomic oxygen on Ag(111), Surf. Sci. 641 (2015) L1–L4.
[49] J.K. Baird, T.R. King, C. Stein, Diffusion of oxygen in silver, J. Phys. Chem. Solids 60 (1999) 891–894.
[50] M.O. Özbek, I. Önal, R.A. van Santen, Ethylene epoxidation catalyzed by silver oxide, ChemCatChem 3 (2011) 150–153.
[51] P.D. Klugherz, P. Harriott, Kinetics of ethylene oxidation on a supported silver catalyst, AIChE J. 17 (1971) 856–866.
[52] P.L. Metcalf, P. Harriott, Kinetics of silver-catalyzed ethylene oxidation, Ind. Eng. Chem. Proc. Des. Dev. 11 (1972) 478–484.
[53] C. Stegelmann, N.C. Schiødt, C.T. Campbell, P. Stoltze, Microkinetic modeling of ethylene oxidation over silver, J. Catal. 221 (2004) 630–649.
[54] C. Liu, D.P. Wijewardena, A. Sviripa, A. Sampath, D.W. Flaherty, C. Paolucci, Computational and experimental insights into reactive forms of oxygen species on dynamic Ag surfaces under ethylene epoxidation conditions, J. Catal. 405 (2022) 445–461.
[55] Z. Tang, T. Chen, K. Liu, H. Du, S.G. Podkolzin, Atomic, molecular and hybrid oxygen structures on silver, Langmuir 37 (2021) 11603–11610.
[56] T. Pu, A. Setiawan, B. Mosevitzky Lis, M. Zhu, M.E. Ford, S. Rangarajan, I.E. Wachs, Nature and reactivity of oxygen species on/in silver catalysts during ethylene oxidation, ACS Catal. 12 (2022) 4375–4381.
[57] P.H. Keijzer, J.E. van den Reijen, C.J. Keijzer, K.P. de Jong, P.E. de Jongh, Influence of atmosphere, interparticle distance and support on the stability of silver on α-alumina for ethylene epoxidation, J. Catal. 405 (2022) 534–544.
[58] R.A. Kemp, Process for preparing ethylene oxide catalysts, US5364826A, 1994.
[59] K.R. Zope, D. Cormier, S.A. Williams, Reactive silver oxalate ink composition with enhanced curing conditions for flexible substrates, ACS Appl. Mater. Interfaces 10 (2018) 3830–3837.
[60] V.V. Boldyrev, Thermal decomposition of silver oxalate, Thermochim. Acta 388 (2002) 63–90.
[61] S.M. Pourmortazavi, S.S. Hajimirsadeghi, I. Kohsari, R. Fareghi Alamdari, M. Rahimi-Nasrabadi, Determination of the optimal conditions for synthesis of silver oxalate nanorods, Chem. Eng. Technol. 31 (2008) 1532–1535.
[62] W. Yang, C. Wang, V. Arrighi, Preparation and characterization of organic silver precursors for conductive ink, Int. J. Electron. Commun. Eng. 12 (2018) 670–677.
[63] K. Kiryukhina, H. Le Trong, P. Tailhades, J. Lacaze, V. Baco, M. Gougeon, F. Courtade, S. Dareys, O. Vendier, L. Raynaud, Silver oxalate-based solders: New materials for high thermal conductivity microjoining, Scr. Mater. 68 (2013) 623–626.
[64] A.L. Patterson, The Scherrer formula for X-ray particle size determination, Phys. Rev. 56 (1939) 978–982.
[65] C. Weidenthaler, Pitfalls in the characterization of nanoporous and nanosized materials, Nanoscale 3 (2011) 792–810.
[66] J. Speder, L. Altmann, M. Bäumer, J.J.K. Kirkensgaard, K. Mortensen, M. Arenz, The particle proximity effect: from model to high surface area fuel cell catalysts, RSC Adv. 4 (2014) 14971–14978.
[67] J. Lu, J.J. Bravo-Suárez, A. Takahashi, M. Haruta, S.T. Oyama, In situ UV–vis studies of the effect of particle size on the epoxidation of ethylene and propylene on supported silver catalysts with molecular oxygen, J. Catal. 232 (2005) 85–95.
[68] P.D. Srinivasan, S.R. Nitz, K.J. Stephens, E. Atchison, J.J. Bravo-Suárez, Modified Harrick reaction cell for in situ/operando fiber optics diffuse reflectance UV–visible spectroscopic characterization of catalysts, Appl. Catal., A 561 (2018) 7–18.
[69] H.A. Alzahrani, J.J. Bravo-Suarez, Operando Raman Spectroscopy Study of Silver Particle Size Effects on Unpromoted Ag/α-Al_2O_3 During Ethylene Epoxidation with Molecular Oxygen, Available at SSRN: https://ssrn.com/abstract=4247785 or http://dx.doi.org/10.2139/ssrn.4247785, 2022.
[70] X.E. Verykios, F.P. Stein, R.W. Coughlin, R.W. Coughlin, Influence of metal crystallite size and morphology on selectivity and activity of ethylene oxidation catalyzed by supported silver, J. Catal. 66 (1980) 368–382.
[71] J.W. Harris, J. Arvay, G. Mitchell, W.N. Delgass, F.H. Ribeiro, Propylene oxide inhibits propylene epoxidation over Au/TS-1, J. Catal. 365 (2018) 105–114.
[72] S.N. Goncharova, E.A. Paukshtis, B.S. Bal'zhinimaev, Size effects in ethylene oxidation on silver catalysts. Influence of support and Cs promoter, Appl. Catal., A 126 (1995) 67–84.
[73] V.I. Bukhtiyarov, I.P. Prosvirin, R.I. Kvon, S.N. Goncharova, B.S. Bal'zhinimaev, XPS study of the size effect in ethene epoxidation on supported silver catalysts, J. Chem. Soc., Faraday Trans. 93 (1997) 2323–2329.
[74] P. Christopher, S. Linic, Shape- and size-specific chemistry of Ag nanostructures in catalytic ethylene epoxidation, ChemCatChem 2 (2010) 78–83.
[75] A.J. Nagy, G. Mestl, D. Herein, G. Weinberg, E. Kitzelmann, R. Schlögl, The correlation of subsurface oxygen diffusion with variations of silver morphology in the silver–oxygen system, J. Catal. 182 (1999) 417–429.
[76] R.A. Outlaw, S.N. Sankaran, G.B. Hoflund, M.R. Davidson, Oxygen transport through high-purity, large-grain Ag, J. Mater. Res. 3 (1988) 1378–1384.
[77] J. Deng, X. Xu, J. Wang, Y. Liao, B. Hong, In situ surface Raman spectroscopy studies of oxygen adsorbed on electrolytic silver, Catal. Lett. 32 (1995) 159–170.
[78] J. Wang, X. Xu, J. Deng, Y. Liao, B. Hong, In situ Raman spectroscopy studies on the methanol oxidation over silver surface, Appl. Surf. Sci. 120 (1997) 99–105.
[79] B. Pettinger, X. Bao, I. Wilcock, M. Muhler, R. Schlögl, G. Ertl, Thermal decomposition of silver oxide monitored by Raman spectroscopy: from AgO units to oxygen atoms chemisorbed on the silver surface, Angew. Chem. Int. Ed. English 33 (1994) 85–86.
[80] I.E. Wachs, In situ Raman spectroscopy studies of catalysts, Top. Catal. 8 (1999) 57–63.
[81] K. Liu, T. Chen, S. He, J.P. Robbins, S.G. Podkolzin, F. Tian, Observation and identification of an atomic oxygen structure on catalytic gold nanoparticles, Angew. Chem., Int. Ed. 56 (2017) 12952–12957.
[82] R.B. Grant, R.M. Lambert, Alkali metal promoters and catalysts: a single-crystal investigation of ethylene epoxidation on cesium-doped silver(111), Langmuir 1 (1985) 29–33.